

# Minimal Hamiltonian deformations as bulk probes of effective non-Hermiticity in Dirac materials

Sergio Pino-Alarcón,<sup>1</sup> Juan Pablo Esparza,<sup>1, 2</sup> and Vladimir Juričić<sup>1</sup>

<sup>1</sup>*Departamento de Física, Universidad Técnica Federico Santa María, Casilla 110, Valparaíso, Chile*

<sup>2</sup>*Instituto de Física, Pontificia Universidad Católica de Valparaíso, Avenida Universidad 331, Curauma, Valparaíso, Chile*

Non-Hermitian (NH) Dirac semimetals describe open gain–loss systems, yet at charge neutrality models featuring real spectrum often look Hermitian-like, with NH effects absorbed into renormalized band parameters. Here we show that a response-based diagnostic of effective non-Hermiticity can be formulated using minimal pseudo-Lorentz-symmetry-breaking deformations, which separate observables that remain captured by parameter redefinitions from those that exhibit irreducible NH structure. For a two-dimensional NH Dirac semimetal in the weak-NH, real-spectrum regime, we analyze Dirac-cone tilt and velocity anisotropy and compute representative probes of spectral structure, quantum geometry, optical response, and viscoelasticity at zero temperature. We find that tilt yields an NH-dependent slope of the density of states that cannot be collapsed to a single effective velocity, while velocity anisotropy can be captured by effective-velocity reparametrization. Furthermore, the quantum metric and collisionless optical conductivities provide NH-insensitive benchmarks (with the nonlinear conductivity symmetry selected), whereas the shear viscosity offers a discriminator through its tensor structure. Our results identify minimal deformations and bulk response channels that enable access to effective non-Hermiticity even when the spectrum remains real.

## I. INTRODUCTION

Non-Hermitian (NH) extensions of quantum many-body systems provide an effective framework for capturing coherent dynamics in the presence of loss, gain, and more general environmental couplings in condensed-matter and synthetic platforms [1–4]. NH Dirac materials [5–11] are a particularly attractive arena for these ideas, given the broad realizations of Dirac quasiparticles in electronic, photonic, and cold-atom settings [12–16]. Furthermore, the hallmark non-Hermitian skin effect (NHSE), the extensive boundary accumulation driven by nonreciprocity and point-gap topology [17–22], is often strongly suppressed in NH Dirac settings where the spectrum is purely real or purely imaginary and the spectrum under periodic boundary conditions fails to enclose a finite spectral area, a condition typically associated with NHSE [23–27]. A central challenge is therefore to determine which NH features leave unambiguous fingerprints in bulk observables accessible to transport and optical probes [2, 3]. In this paper, we show that a response-based diagnostic of effective non-Hermiticity can be formulated using minimal pseudo-Lorentz-symmetry-breaking deformations, which separate observables that remain captured by parameter redefinitions from those that exhibit irreducible NH structure.

Non-Hermiticity makes the problem subtle because it can enter observables through two distinct mechanisms. In one route, it acts at the level of the spectrum, producing complex energies, exceptional degeneracies, and the accompanying nonanalytic features [28, 29]. In the other, the spectrum may remain entirely real, as in the weak-NH regime, yet the eigenstates are nonetheless altered, so that response functions probe the underlying biorthog-

onal wave-function structure [30, 31]. Crucially, these two effects do not have to track each other in bulk measurements: depending on whether a probe is controlled primarily by spectral properties or by the wave-function structure, it can be highly sensitive to one manifestation of non-Hermiticity while remaining largely insensitive to the other.

This challenge is especially pertinent at charge neutrality, where symmetry and the Dirac band structure often enforce universal response coefficients. In particular, in minimal weak-NH Dirac models with real spectra several bulk responses remain effectively NH insensitive: non-Hermiticity can be absorbed into a renormalization of band parameters (e.g., an effective Dirac velocity), so that standard observables fail to provide independent access to NH couplings [5]. Put differently, response functions can mask the microscopic origin of non-Hermiticity, yielding results indistinguishable from those of a purely Hermitian theory with a suitably reparametrized band structure. A guiding principle in this work is scaling: in the collisionless regime at charge neutrality, relevant for Dirac semimetals, the dynamic exponent  $z = 1$  and spatial dimensionality  $d = 2$  fix the leading power-law behavior of the responses, so the central issue is not the exponent itself but whether non-Hermiticity leaves irreducible, response-dependent prefactors or tensor structures that survive any reparametrization. This motivates the search for minimal, symmetry-allowed perturbations and a set of experimentally accessible observables for which NH parameters enter bulk response in a way that cannot be reduced to such parameter redefinitions.

Observable	Scaling	Tilt deformation	VAD	Where
$\rho(E)$	$\sim  E $	$\sim f_{\text{tilt}}(\alpha, \beta)$	$\sim (v_x^{\text{eff}} v_y^{\text{eff}})^{-1}$	Sec. II
$Q_{\mu\nu}(k)$	$\sim k^{-2}$	$= Q_{\mu\nu}^{(0)}$	$= Q_{\mu\nu}(v_x^{\text{eff}}, v_y^{\text{eff}})$	Sec. III
$\sigma_{ij}^{(1)}(\omega)$	$\sim \omega^0$	$\sigma_{xx}^{(1)} = \sigma_{yy}^{(1)} = \sigma_0$	$\sigma_{xx}^{(1)} = (v_x^{\text{eff}}/v_y^{\text{eff}})\sigma_0$ $\sigma_{yy}^{(1)} = (v_y^{\text{eff}}/v_x^{\text{eff}})\sigma_0$	Sec. IV A
$\sigma_{ijk}^{(2)}(\omega_1, \omega_2)$	$\sim (\omega_1 \omega_2)^{-1}$	$\neq 0$ (inversion odd)	$= 0$ (inversion even)	Sec. IV B
$\eta_{\alpha\beta\gamma\delta}(\omega)$	$\sim \omega^2$	$= \eta_0(\omega) P_{\alpha\beta\gamma\delta}$	inequivalent components	Sec. V

TABLE I. Behavior of the observables in a deformed two-dimensional ( $d = 2$ ) non-Hermitian Dirac semimetal at zero temperature ( $T = 0$ ) with the dynamical exponent  $z = 1$ : scaling exponents of observables are fixed by  $(d, z)$  while diagnostic content is in prefactors and tensor structure. Non-Hermiticity-insensitive benchmarks are given by quantum geometric tensor  $[Q_{\mu\nu}(k)]$  with  $Q_{\mu\nu}^{(0)}(k)$  being the form for the undeformed Dirac Hamiltonian, Eq. (17)], and linear optical conductivity ( $\sigma^{(1)}(\omega)$ ). Non-Hermiticity-sensitive fingerprints are slope of the density of states ( $\rho(E)$ ) for tilt deformation and viscosity tensor ( $\eta_{\alpha\beta\gamma\delta}(\omega)$ ) for velocity-anisotropic deformation (VAD). See Eqs. (34) and (35). The last column indicates the section in which each observable is discussed.

### A. Summary of the results

Here we show that minimal Hamiltonian deformations provide precisely such a controlled setting by sharply distinguishing responses that collapse under parameter redefinitions from those that retain irreducible NH structure, as also summarized in Table I. In Dirac and Weyl materials, the simplest departures from a perfectly pseudo-Lorentz-invariant cone, most notably a tilt term [32–38] and velocity-anisotropy deformation (VAD) [39–45], are ubiquitous already in Hermitian systems. Their impact is apparent already at the level of basic spectral features. In both cases the density of states remains linear,  $\rho(E) \sim |E|$  but the origin of the slope is different: a tilt deformation can imprint an effective non-Hermiticity in the prefactor, whereas the VAD implements a controlled anisotropic deformation of the Dirac cone, equivalently introducing distinct direction-dependent effective velocities  $v_x^{\text{eff}}$  and  $v_y^{\text{eff}}$ . As a result, the DOS for VAD is insensitive to non-Hermiticity since it is modified through an anisotropic velocity rescaling.

A natural candidate for a complementary, wavefunction-sensitive diagnostic of non-Hermiticity is the biorthogonal quantum geometric tensor (QGT), which extends the quantum metric and Berry curvature to non-Hermitian band structures [46–54]. However, as we here show, in the weak-NH, real-spectrum regime, the quantum metric is insensitive to non-Hermiticity for both deformations considered here. For tilt, the eigenstate geometry is unchanged, so the QGT remains identical to its untilted form. Velocity anisotropy is likewise QGT-insensitive to non-Hermiticity in this regime: it modifies the QGT in the way already present in the Hermitian problem, without any additional dependence on the non-Hermitian coupling beyond what can be absorbed into effective anisotropic velocities. This stands in sharp contrast to the DOS, whose linear form is universal but its slope can already acquire a genuine NH dependence for the tilt deformation.

With this structure in place, we turn to bulk response functions. In Sec. IV we compute the collisionless lin-

ear and second-order optical conductivities and show that the linear response is NH-insensitive: for the tilt it remains universal, while for the VAD it reduces to the standard anisotropic-Dirac form through a simple reparametrization in terms of effective velocities. The second-order conductivity is symmetry-selected, vanishing unless inversion symmetry is broken, and is therefore nonzero only for the tilt deformation (breaking this symmetry). We then consider stress-response observables in Sec. V, where the optical shear viscosity offers a complementary window on non-Hermiticity through its tensorial structure. In particular, we find that the shear viscosity is anisotropic with multiple independent components for the velocity-anisotropy deformation (VAD), whereas it collapses to an isotropic projector form for the tilted NH Dirac Hamiltonian. This identifies the DOS and viscoelastic response as natural bulk diagnostics, where minimal deformations reveal effective non-Hermiticity.

### B. Organization

Our paper is organized as follows. In Sec. II we introduce the NH Dirac model with minimal deformations realizing the tilt and the VAD, and discuss the DOS for both deformations. In Sec. III we analyze the biorthogonal QGT as a possible NH diagnostic. In Sec. IV we turn to optical response and compute the collisionless linear and second-order conductivities where we show that both are NH-insensitive. In Sec. V we study the optical shear viscosity and show that stress response provides a complementary probe of non-Hermiticity: it is anisotropic with multiple independent components for VAD, but collapses to an isotropic projector form for tilted NH Dirac Hamiltonian. Finally, Sec. VI summarizes our results and discusses natural extensions. Technical details are presented in the Appendices.

## II. MODEL

We consider a minimal continuum description of a two-dimensional Dirac semimetal at charge neutrality in the presence of weak non-Hermiticity. The low-energy degrees of freedom are collected into a four-component spinor  $\Psi_{\mathbf{k}}$ , which in microscopic realizations can be viewed as carrying sublattice and valley flavors for spinless Dirac materials (e.g., graphene) [55]. Throughout we set  $\hbar = 1$  and work at  $T = 0$  unless stated otherwise.

The Hermitian Dirac Hamiltonian reads  $\mathcal{H}_D = \sum_{\mathbf{k}} \Psi_{\mathbf{k}}^{\dagger} H_D(\mathbf{k}) \Psi_{\mathbf{k}}$ , with

$$H_D(\mathbf{k}) = v_{\text{H}} h_0(\mathbf{k}), \quad (1)$$

where the operator

$$h_0(\mathbf{k}) = \Gamma_x k_x + \Gamma_y k_y, \quad (2)$$

and the Dirac matrices obey the Clifford algebra  $\{\Gamma_i, \Gamma_j\} = 2\delta_{ij}$  ( $i, j = x, y$ ). The spinor  $\Psi_{\mathbf{k}}$  is model dependent; for definiteness we take it to be four-component, as in graphene with two sublattice and two valley degrees of freedom. We choose the Hermitian representation  $\Gamma_x = \sigma_1 \otimes \tau_3$  and  $\Gamma_y = \sigma_2 \otimes \tau_0$ , where  $(\sigma_0, \sigma) [(\tau_0, \tau)]$  act in sublattice (valley) space. All final results depend only on the Clifford algebra and are therefore representation independent.

A minimal NH extension is generated by a Hermitian matrix  $M$  that anticommutes with  $h_0$ ,  $\{M, h_0\} = 0$ , so that  $M h_0$  is anti-Hermitian [5]. Introducing the dimensionless NH parameter  $\beta \equiv v_{\text{NH}}/v_{\text{H}} \in \mathbb{R}$ , we write

$$H_{\text{NH}}(\mathbf{k}) = v_{\text{H}} (1 + \beta M) h_0(\mathbf{k}). \quad (3)$$

The spectrum is

$$E_{\text{NH}}(\mathbf{k}) = \pm v_{\text{F}} |\mathbf{k}|, \quad (4)$$

with the effective Fermi velocity

$$v_{\text{F}} = v_{\text{H}} \sqrt{1 - \beta^2}, \quad (5)$$

which is purely real for  $|\beta| < 1$ . We focus on this weak-NH regime, where non-Hermiticity primarily enters through the biorthogonal structure of eigenstates. For concreteness, we here choose  $M = \sigma_3 \otimes \tau_3$  to ensure spatial inversion symmetry of  $H_{\text{NH}}$ , represented by  $I = \sigma_1 \otimes \tau_1$ , featured by its Hermitian counterpart in Eq. (1). Importantly, many standard bulk responses at charge neutrality can then be mapped to Hermitian forms by the replacement  $v_{\text{H}} \rightarrow v_{\text{F}}$  [5] which hinders the detection of non-Hermiticity; one of our goals is to identify minimal deformations and observables that can evade this limitation.

### A. Minimal deformation terms: Tilt and velocity anisotropy

To break pseudo-Lorentz symmetry without opening a gap, we add a (real) deformation term linear in  $k_x$ ,

$$\begin{aligned} H_{\text{NH}}^{\text{def}}(\mathbf{k}) &= v_{\text{H}} \left[ (1 + \beta M) h_0(\mathbf{k}) + \alpha T k_x \right] \\ &\equiv H_{\text{NH}}(\mathbf{k}) + H_{\text{def}}(\mathbf{k}), \end{aligned} \quad (6)$$

where  $\alpha$  is a dimensionless parameter. Crucially, the character of the deformation is encoded in the commutation relation between the deformation matrix  $T$  and the NH Dirac Hamiltonian. A tilt corresponds to a commuting deformation,  $[T, H_{\text{NH}}(\mathbf{k})] = 0$ , which can be realized, for example, by choosing  $T = \sigma_0 \otimes \tau_0$ . In this case the tilt acts as a momentum-dependent chemical potential, leading to the spectrum

$$E_{\text{NH}}^{\text{tilt}}(\mathbf{k}) = \pm v_{\text{F}} |\mathbf{k}| + \alpha v_{\text{H}} k_x, \quad (7)$$

and throughout we restrict to the type-I regime  $\alpha^2 + \beta^2 < 1$ , where charge neutrality coincides with a nodal point. This deformation breaks spatial inversion symmetry of  $H_{\text{NH}}$  in Eq. (3), but the symmetry of the tilt deformation plays no role in our analysis except for the second-order optical conductivity (Sec. IV B).

On the other hand, the VAD is defined by the matrix anticommuting with NH Hamiltonian,  $\{T, H_{\text{NH}}(\mathbf{k})\} = 0$ , with the spectrum effectively becoming anisotropic close to each Dirac cone,

$$E_{\text{NH}}^{\text{VAD}}(\mathbf{k}) = \pm \sqrt{(v_x^{\text{eff}})^2 k_x^2 + (v_y^{\text{eff}})^2 k_y^2}, \quad (8)$$

where the effective velocity in the  $x$ -( $y$ -)direction is  $v_x^{\text{eff}} = v_{\text{H}} \sqrt{1 + \alpha^2 - \beta^2}$  ( $v_y^{\text{eff}} = v_{\text{H}} \sqrt{1 - \beta^2}$ ), and we consider the regime  $|\beta| < 1$  ensuring the purely real spectrum of the deformed NH Hamiltonian. With the stage being set, we now turn to the analysis of the DOS.

### B. Density of states

We compute the density of states (DOS) from the retarded Green's function,

$$\rho(E) = -\frac{1}{\pi} \text{Im} \int_{\mathbf{k}} \text{Tr} G^{\text{def}, R}(E, \mathbf{k}), \quad (9)$$

with  $\int_{\mathbf{k}} \equiv \int \frac{d^2 \mathbf{k}}{(2\pi)^2}$  and  $G^{\text{def}, R}(E, \mathbf{k})$  obtained by analytic continuation  $i\omega \rightarrow E + i\eta$ , in the limit  $\eta \rightarrow 0^+$ , of the Matsubara Green's function corresponding to the deformed NH Dirac Hamiltonian in Eq. (6), given by

$$G^{\text{def}}(i\omega, \mathbf{k}) \equiv [i\omega - H_{\text{NH}}^{\text{def}}(\mathbf{k})]^{-1}, \quad (10)$$

which implies the universal scaling form of the DOS,  $\rho(E) \sim |E|^{\frac{d}{z}-1} f_{\rho}$ , where  $f_{\rho}$  is a dimensionless scaling

function of the dimensionless variables that depend on the form of the Hamiltonian. Therefore, in  $d = 2$  and for the Dirac system featuring the linear energy-momentum dispersion, implying  $z = 1$ , this scaling form reduces to  $\rho(E) \sim |E|f_\rho$ .

We first consider the closed the tilt deformation yielding the Green's function in the form

$$G^{\text{tilt}}(i\omega, \mathbf{k}) = \left[ (i\omega + H_{\text{NH}}) A_+ - B \hat{v}_M(\mathbf{\Gamma} \cdot \mathbf{k}) T k_x \right. \\ \left. - 2\alpha v_F k_x \left( v_F^2 k^2 T + \alpha v_H k_x \hat{v}_M(\mathbf{\Gamma} \cdot \mathbf{k}) \right) \right] \frac{1}{B^2 - A_-^2}. \quad (11)$$

Here,  $H_{\text{NH}}$  is given in Eq. (3),  $\hat{v}_M \equiv v_H + v_{\text{NH}}M$ , and

$$A_\pm = \omega^2 + v_F^2 k^2 \pm \alpha^2 v_H^2 k_x^2, \quad B = 2i\alpha v_H \omega k_x, \quad (12)$$

with  $k \equiv |\mathbf{k}|$  and  $v_F = v_H \sqrt{1 - \beta^2}$ .

At charge neutrality the DOS remains linear,  $\rho(E) \sim |E|$ , as expected for a subcritical Dirac cone, with the explicit form [56]

$$\rho_{\text{tilt}}(E) = N_f \frac{|E|}{\pi(v_F^{\text{tilt}})^2} \sqrt{\frac{1 - \beta^2}{1 - \alpha^2 - \beta^2}}, \quad (13)$$

with  $v_F^{\text{tilt}} = v_H \sqrt{1 - \alpha^2 - \beta^2}$ , and  $N_f$  is the number of four-component fermion species. Equation (13) already shows that the DOS is consistent with the expected scaling form but its slope depends on  $\alpha$  and  $\beta$  in a way that is not captured by  $v_F^{\text{tilt}}$  alone therefore representing an NH sensitive observable. Finally, in the limit  $\alpha \rightarrow 0$ , the DOS reduces to the form for the deformation-free Hamiltonian with the NH parameter absorbed in the effective Fermi velocity.

For the VAD, the DOS provides a simple illustration of NH insensitivity in the real-spectrum regime. The deformation breaks isotropy by assigning different velocities along the two directions (see Eq. (8)), with the Green's function of the form,

$$G^{\text{VAD}}(i\omega, \mathbf{k}) = -\frac{i\omega + H_{\text{NH}}^{\text{VAD}}}{\omega^2 + (E_{\text{NH}}^{\text{VAD}}(\mathbf{k}))^2}, \quad (14)$$

where  $H_{\text{NH}}^{\text{VAD}}$  is given by Eq. (6) with the matrix  $T$  anticommuting with the NH Dirac Hamiltonian [Eq. (3)], yielding the DOS

$$\rho(E) = N_f \frac{|E|}{\pi v_x^{\text{eff}} v_y^{\text{eff}}}. \quad (15)$$

Since the electronic bands are still described by an anisotropic Dirac cone, the DOS preserves its universal linear scaling,  $\rho(E) \sim |E|$ . Crucially, any dependence on the NH coupling can be absorbed into a redefinition of direction-dependent effective velocities,  $v_x^{\text{eff}}$  and  $v_y^{\text{eff}}$ , so that the resulting expression is identical to the DOS of an ordinary Hermitian anisotropic Dirac Hamiltonian. In this sense, VAD reshapes the DOS prefactor purely kinematically, by changing the effective velocities, without generating a distinct fingerprint of non-Hermiticity in this observable.

### III. QUANTUM GEOMETRIC TENSOR

While spectral diagnostics such as the DOS are fixed by the single-particle spectrum, they do not access the geometric information carried by the eigenvectors, i.e., the Hilbert-space embedding of the bands. We therefore begin with a wave-function-sensitive quantity: the biorthogonal quantum geometric tensor (QGT), which generalizes the quantum metric and Berry curvature to NH band structures [46, 57, 58]. In the weak-NH, real-spectrum regime considered here, the QGT directly diagnoses whether a given tilt realization reshapes the left/right eigenstates and thus whether non-Hermiticity leaves an irreducible imprint beyond parameter renormalizations. Importantly, the QGT is gauge invariant under smooth, momentum-dependent  $U(1)$  transformations of the biorthogonal eigenstates that preserve the chosen normalization, and it can be expressed entirely in terms of the associated band projector. It therefore provides a sharp, representation-independent notion of geometry of the Hilbert space for NH bands, even though the right/left eigenvectors need not be related by any unitary transformation.

For band  $n$  we define the QGT as

$$Q_{\mu\nu}^n = \langle \partial_\mu \psi_n^L | \partial_\nu \psi_n^R \rangle - \langle \partial_\mu \psi_n^L | \psi_n^R \rangle \langle \psi_n^L | \partial_\nu \psi_n^R \rangle, \quad (16)$$

where  $|\psi_n^{R/L}\rangle$  are right/left eigenstates of  $H_{\text{NH}}^{\text{tilt}}(\mathbf{k})$  and  $\partial_\mu \equiv \partial/\partial k_\mu$  with  $\mu, \nu \in \{x, y\}$ . The real symmetric part,  $g_{\mu\nu}^n \equiv \text{Re } Q_{\mu\nu}^n$ , defines the (biorthogonal) quantum metric, which controls the infinitesimal distance between nearby Bloch states in momentum space, while the imaginary antisymmetric part,  $\Omega_{\mu\nu}^n \equiv -2 \text{Im } Q_{\mu\nu}^n$ , plays the role of a (biorthogonal) Berry curvature. In the present work we focus on the metric sector, since it provides the most direct diagnostic of whether tilt reshapes the eigenstates in a way that is invisible to eigenvalue-only quantities.

In the untilted case the QGT is rotationally invariant and, in Cartesian coordinates, takes the form

$$\hat{Q} = \frac{1}{4(k_x^2 + k_y^2)^2} \begin{pmatrix} k_y^2 & -k_x k_y \\ -k_x k_y & k_x^2 \end{pmatrix}, \quad (17)$$

for both conduction and valence bands. Notably, Eq. (17) is independent of velocity parameters, so the replacement  $v_H \rightarrow v_F$  leaves the QGT unchanged. Equivalently, upon transforming to polar coordinates  $(k, \varphi)$ , the only nonzero component is  $Q_{\varphi\varphi} = 1/4$ . This purely angular quantum geometry can be viewed as a direct imprint of the scale (and fixed-point conformal) structure of the massless Dirac Hamiltonian, as follows. At charge neutrality the eigenprojectors depend only on the direction  $\hat{\mathbf{k}} = \mathbf{k}/|\mathbf{k}|$  and are invariant under the scale transformation  $\mathbf{k} \rightarrow \lambda \mathbf{k}$ , which rescales the spectrum but leaves the eigenstates unchanged. Consequently, radial derivatives of the Bloch spinors vanish and the quantum metric has no radial components,  $Q_{kk} = Q_{k\varphi} = 0$ , while  $Q_{\varphi\varphi} = 1/4$

is fixed by the geometry of the Dirac cone as directly obtained from Eq. (17). In this sense the quantum geometry is entirely angular and independent of the radial component of momentum  $k$ , consistent with the underlying scale invariance of the Dirac Hamiltonian.

Turning on the tilt, we find that the eigenstate geometry is unaffected: the tilt term acts as a purely spectral deformation that leaves the band projectors unchanged. Consequently, the right/left eigenvectors coincide with those of the untilted model and the QGT remains identical to Eq. (17), consistent with Ref. [59]. Put differently, tilt shifts the dispersion without rotating the pseudospin texture, so the Hilbert-space embedding of the bands is unmodified even though the single-particle energies are affected by the tilt term.

For the velocity-anisotropic Hamiltonian, the deformation reshapes the eigenstates and the QGT takes the form

$$\hat{Q}_{\text{VAD}} = \frac{(1 - \beta^2)(1 - \beta^2 + \alpha^2)}{4[(1 - \beta^2)k^2 + \alpha^2 k_x^2]^2} \begin{pmatrix} k_y^2 & -k_x k_y \\ -k_x k_y & k_x^2 \end{pmatrix}. \quad (18)$$

That is, the matrix part retains the usual Dirac structure, while the prefactor encodes the deformation. In particular, the prefactor makes the geometry explicitly anisotropic, with the degree of anisotropy controlled by  $\alpha$ , and the overall scale modulated by the NH coupling  $\beta$ . This form (Eq. (18)) reduces smoothly to the quantum metric in the undeformed case, given by Eq. (17), as  $\alpha \rightarrow 0$ . Moreover, for any finite deformation its  $\beta$ -dependence can be re-expressed as a rescaling of effective velocities along the two directions (Eq. (8)). In this sense, the resulting quantum metric is indistinguishable from that of a Hermitian Dirac semimetal with anisotropic velocities. Thus, within the minimal real-spectrum Dirac models, the QGT does not furnish a direct bulk diagnostic of effective non-Hermiticity: its NH dependence can be absorbed into velocity renormalizations rather than producing a distinct geometric imprint.

#### IV. OPTICAL CONDUCTIVITIES

We next turn to optical response in the collisionless regime at charge neutrality and  $T = 0$ , where interband particle-hole excitations dominate and the corresponding optical conductivities assume universal forms. We compute the linear and second-order conductivities for both minimal deformations considered here, and show that they provide NH-insensitive benchmarks.

##### A. Linear optical conductivity

We compute the collisionless linear optical conductivity using the Kubo formula. Coupling to an external electromagnetic field via minimal substitution,  $\mathbf{k} \rightarrow \mathbf{k} - e\mathbf{A}$  (setting  $\hbar = 1$ ), the Bloch Hamiltonian becomes

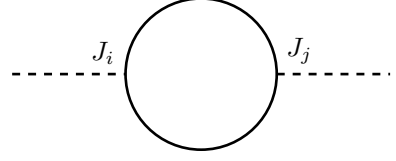


FIG. 1. Polarization diagram corresponding to Eq. (20). Here, a solid line denotes the Dirac fermion propagator, a dashed line corresponds to the external electromagnetic potential, while the vertex corresponds to the current as dictated by the U(1) gauge invariance.

$H(\mathbf{k} - e\mathbf{A})$ . Expanding to linear order in  $\mathbf{A}$  defines the current operator

$$J_i(\mathbf{k}) \equiv - \frac{\partial H(\mathbf{k} - e\mathbf{A})}{\partial A_i} \Big|_{\mathbf{A}=0} = e \frac{\partial H(\mathbf{k})}{\partial k_i} \equiv e v_i(\mathbf{k}), \quad (19)$$

with  $v_i$  the velocity operator and  $i \in \{x, y\}$ . The linear conductivity is obtained from the polarization (current-current correlator) at  $T = 0$ , with the corresponding Feynman diagram in Fig. 1, which reads as

$$\Pi_{ij}(i\Omega) = - \int_{\nu, \mathbf{k}} \text{Tr} [J_i(\mathbf{k}) G(i\nu, \mathbf{k}) J_j(\mathbf{k}) G(i\nu + i\Omega, \mathbf{k})], \quad (20)$$

where  $\int_{\nu, \mathbf{k}} \equiv \int \frac{d\nu d^2 k}{(2\pi)^3}$  and  $G(i\omega, \mathbf{k}) = [i\omega - H(\mathbf{k})]^{-1}$  is the (biorthogonal) single-particle Green's function. After analytic continuation  $i\Omega \rightarrow \omega + i\eta$ , with  $\eta \rightarrow 0^+$ , the collisionless conductivity follows from the retarded correlator as

$$\sigma_{ab}(\omega) = \frac{1}{\omega} \text{Im} \Pi_{ab}^R(\omega), \quad (21)$$

evaluated at charge neutrality and  $T = 0$ , where only interband particle-hole processes contribute. The U(1) gauge invariance of the electromagnetic coupling then implies that the linear optical conductivity has the engineering scaling dimension  $\text{dim}[\sigma_{ab}] = d - 2$ , implying that it is dimensionless in  $d = 2$ , and thus universal for the undeformed Dirac Hamiltonian, with the value

$$\sigma_0 = N_f \frac{\pi}{4} \quad (22)$$

in units  $e^2/h$  [60].

For the tilt deformation the longitudinal optical conductivity retains its universal form, which is independent of  $\alpha$  and  $\beta$ , as for the Hermitian Dirac Hamiltonian,

$$\sigma_{xx}(\omega) = \sigma_{yy}(\omega) = \sigma_0. \quad (23)$$

Thus, in the collisionless interband regime, the longitudinal linear optical conductivity provides an NH-insensitive response even in the presence of tilt.

For the VAD, the longitudinal optical conductivity is no longer strictly universal, but it remains NH-insensitive in the sense that it can be written in the standard

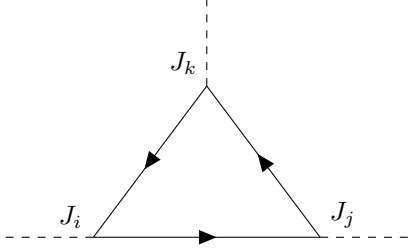


FIG. 2. Second-order susceptibility (triangle) diagram corresponding to Eq. (27) yielding the second-order optical conductivity. The labels are the same as in Fig. 1.

anisotropic-Dirac form, with non-Hermiticity entering only through the effective velocities,

$$\begin{aligned}\sigma_{xx}(\omega) &= \sigma_0 \mathcal{F}(\alpha, \beta), \\ \sigma_{yy}(\omega) &= \sigma_0 \mathcal{F}(\alpha, \beta)^{-1},\end{aligned}\quad (24)$$

in units of  $e^2/h$ , where

$$\mathcal{F}(\alpha, \beta) = \sqrt{\frac{1 + \alpha^2 - \beta^2}{1 - \beta^2}} = \frac{v_x^{\text{eff}}}{v_y^{\text{eff}}}. \quad (25)$$

Thus, unlike the tilt deformation, which preserves the universal value  $\sigma_0$ , the VAD introduces anisotropy through an overall velocity ratio, with all dependence on the anisotropy and NH parameters absorbed into the single combination  $v_x^{\text{eff}}/v_y^{\text{eff}}$ . In this way, the VAD optical response maps directly onto that of a generic (Hermitian or NH) anisotropic Dirac semimetal, for which anisotropy appears as  $\sigma_{xx} = \sigma_0 v_y/v_x$  and  $\sigma_{yy} = \sigma_0 v_x/v_y$ , and hence  $\sigma_{xx} \neq \sigma_{yy}$  unless  $v_x = v_y$ .

## B. Second-order optical conductivity

For completeness, we next analyze the second-order optical response at charge neutrality and  $T = 0$ . In the collisionless regime the second-order conductivity tensor follows from the three-current Kubo formula [61, 62],

$$\sigma_{ijk}^{(2)}(\omega_1, \omega_2) = - \lim_{\eta \rightarrow 0^+} \sum'_{\mathcal{P}} \frac{\chi_{ijk}^{(2)}(i\Omega_1, i\Omega_2)}{\omega_1 \omega_2} \Bigg|_{i\Omega_s \rightarrow \omega_s + i\eta}, \quad (26)$$

where  $\sum'_{\mathcal{P}}$  symmetrizes under  $(j, \omega_1) \leftrightarrow (k, \omega_2)$  and the corresponding susceptibility, with the Feynman diagram shown in Fig. 2, reads

$$\begin{aligned}\chi_{ijk}^{(2)}(i\Omega_1, i\Omega_2) &= \sum_{\mathcal{P}} \int_{\omega, \mathbf{k}} \text{Tr} \left[ J_i(\mathbf{k}) G(i\omega, \mathbf{k}) J_j(\mathbf{k}) \right. \\ &\quad \times \left. G(i\omega + i\Omega_1, \mathbf{k}) J_k(\mathbf{k}) G(i\omega + i\Omega_1 + i\Omega_2, \mathbf{k}) \right].\end{aligned}\quad (27)$$

This form of the susceptibility, together with the Kubo formula (26), implies the universal scaling form of the

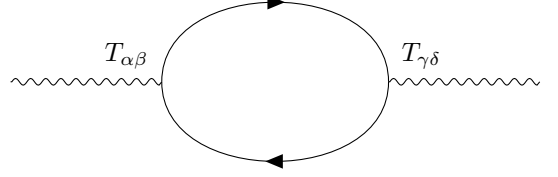


FIG. 3. Feynman diagram corresponding to the stress correlator in Eq. (32) determining the optical shear viscosity. Solid lines denote Dirac fermion propagators, wavy lines represent external strain tensor, while the vertex corresponds to the stress tensor.

second-order optical conductivity for a two-dimensional ( $d = 2$ ) system with the dynamical exponent  $z = 1$ , is  $\sigma_{ijk}^{(2)}(\omega_1, \omega_2) = (\omega_1 \omega_2)^{-1} f_{\sigma_2}$ , where  $f_{\sigma_2}$  is a universal dimensionless scaling function of the dimensionless variables [63]. Furthermore, for this observable, the spatial inversion symmetry, represented by the matrix  $I = \sigma_1 \otimes \tau_1$  for the NH Dirac Hamiltonian in Eq. (3) acts as a sharp symmetry diagnostic [64]. The tilt deformation, being odd under inversion allows a transverse nonlinear current,

$$\sigma_{\text{tilt}, yjk}^{(2)}(\omega_1, \omega_2) = -\frac{i N_f e^3 \alpha v_H}{4 \omega_1 \omega_2} \varepsilon_{jk}, \quad (28)$$

with  $\varepsilon_{jk}$  being completely antisymmetric symbol, while the remaining components of the conductivity tensor are vanishing. See Appendix A for technical details. On the other hand, for the inversion-symmetric VAD, represented by  $T = \sigma_3 \otimes \tau_0$  for the choice of  $M = \sigma_3 \otimes \tau_3$  in the NH Dirac Hamiltonian (3),

$$\sigma_{\text{VAD}, ijk}^{(2)}(\omega_1, \omega_2) = 0. \quad (29)$$

Therefore, for minimal deformations considered here, the nonlinear response is controlled by the symmetry of the deformation term and its magnitude, while remaining independent of the NH strength  $\beta$ , providing a second NH-insensitive optical response.

## V. SHEAR VISCOSITY

We finally analyze the dynamical (optical) shear viscosity in the collisionless regime at  $T = 0$ . Unlike the optical conductivities in the minimal theory, the stress response is intrinsically sensitive to a reduction of rotational symmetry and to how the NH deformation reshapes the underlying biorthogonal structure, and it therefore provides a natural setting in which deformation-dependent NH effects may enter bulk response [65–73].

We define the stress tensor operator as [66]

$$T_{\alpha\beta}(\mathbf{k}) = -i [H(\mathbf{k}), \mathcal{J}_{\alpha\beta}], \quad (30)$$

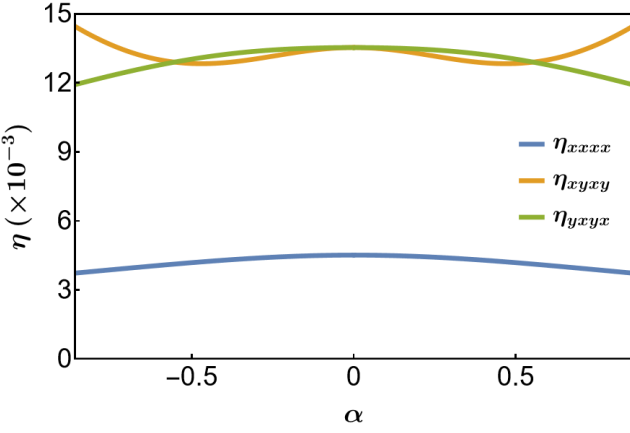


FIG. 4. Components of the shear viscosity tensor for the symmetric tilt realization with varying  $\alpha$  at fixed  $\beta = 0.5$  at frequency  $\Omega = 1$ . We here fix  $v_H = 1$  and  $N_f = 1$ .

where  $\mathcal{J}_{\alpha\beta} = \mathcal{L}_{\alpha\beta} + S_{\alpha\beta}$  is the total angular momentum,  $\mathcal{L}_{\alpha\beta} = -x_\alpha k_\beta$  is orbital angular momentum, and  $S_{\alpha\beta}$  generates pseudospin rotations. The orbital part yields

$$T_{\alpha\beta}^{(o)}(\mathbf{k}) = k_\beta \frac{\partial H(\mathbf{k})}{\partial k_\alpha}. \quad (31)$$

and in the pseudospin sector one may take  $S_{ij} = -(1/4)\varepsilon_{ijz}\sigma_z$ . The (Matsubara) stress correlator is

$$C_{\alpha\beta\gamma\delta}(i\Omega) = - \int_{-\infty}^{\infty} \frac{d\omega}{2\pi} \int \frac{d^2\mathbf{k}}{(2\pi)^2} \text{Tr} \left[ G(i\omega, \mathbf{k}) T_{\alpha\beta}(\mathbf{k}) \times G(i\omega + i\Omega, \mathbf{k}) T_{\gamma\delta}(\mathbf{k}) \right], \quad (32)$$

with the Feynman diagram shown in Fig. 3, and the optical viscosity follows from analytic continuation,

$$\eta_{\alpha\beta\gamma\delta}(\Omega) = \lim_{\delta \rightarrow 0^+} \frac{1}{\Omega} \text{Im} \left[ C_{\alpha\beta\gamma\delta}(i\Omega \rightarrow \Omega + i\delta) \right], \quad (33)$$

which, together with Eq. (32), implies the engineering scaling dimension of the shear viscosity  $\dim[\eta_{\alpha\beta\gamma\delta}] = d$ , and therefore in  $d = 2$  for a theory featuring dynamical exponent  $z = 1$ ,  $\eta_{\alpha\beta\gamma\delta}(\Omega) = \Omega^2 \mathcal{G}_{\alpha\beta\gamma\delta}$ , with  $\mathcal{G}_{\alpha\beta\gamma\delta}$  as the dimensionless function of the dimensionless variables which is determined by the details of the Hamiltonian.

Turning first to the VAD, the viscosity develops a genuinely anisotropic multi-component structure with explicit dependence on  $\alpha$  and  $\beta$ ,

$$\begin{aligned} \eta_{V,\rho\rho\rho\rho}(\Omega) &= -\eta_{V,\rho\rho\sigma\sigma}(\Omega) = -\eta_{V,\sigma\rho\rho\sigma}(\Omega) = \Omega^2 f_1(\alpha, \beta), \\ \eta_{V,xyxy}(\Omega) &= \Omega^2 f_2(\alpha, \beta), \quad \eta_{V,yxyx}(\Omega) = \Omega^2 f_3(\alpha, \beta), \end{aligned} \quad (34)$$

where  $\rho, \sigma \in \{x, y\}$  with  $\sigma \neq \rho$ , and explicit forms of functions  $f_i$ , are given in Appendix B. The decomposition in Eq. (34) makes transparent that, for VAD, the shear viscosity tensor contains several independent components already at the level of collisionless response. The

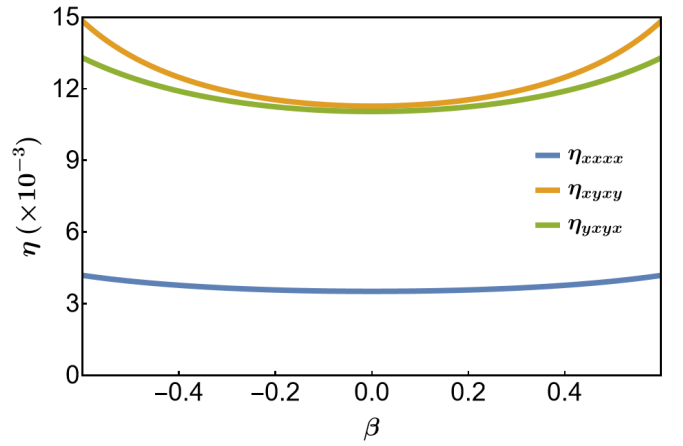


FIG. 5. Components of the shear viscosity tensor for the symmetric tilt realization with varying  $\beta$  at fixed  $\alpha = 0.7$  at frequency  $\Omega = 1$ . We here fix  $v_H = 1$  and  $N_f = 1$ .

VAD reduces rotational symmetry and the resulting viscoelastic response is no longer characterized by a single scalar function, but by a set of inequivalent tensor components with amplitudes depending on both  $\alpha$  and  $\beta$ .

This structure is illustrated in Fig. 4, which shows representative components as a function of the VAD strength  $\alpha$  at fixed NH parameter  $\beta$ . The curves are even in  $\alpha$ , as expected since the effective velocities are also even in this parameter. Importantly, the difference between the shear components  $\eta_{xyxy}$  and  $\eta_{yxyx}$  provides a direct diagnostic of broken rotational invariance in the stress response. In a rotationally invariant Dirac theory these components are constrained to coincide; in the presence of the VAD, they become inequivalent, reflecting the deformation-induced anisotropy of the underlying biorthogonal structure.

For comparison, Fig. 5 displays the same components as a function of the non-Hermiticity strength  $\beta$  at fixed  $\alpha$ . In this cut, the evolution with  $\beta$  isolates the genuinely NH-sensitive part of the stress response: increasing  $|\beta|$  amplifies the anisotropic shear sector and drives an overall enhancement that becomes strongest as one approaches the edge of the real-spectrum regime. Therefore, for VAD, shear viscosity represents a bulk probe of non-Hermiticity, which in the limit of vanishing deformation,  $\alpha \rightarrow 0$ , reduces to the result for the NH Dirac Hamiltonian, given by Eq. (37).

By contrast, for the tilted NH Dirac Hamiltonian the response collapses to an isotropic form form,

$$\eta_{\text{tilt},\alpha\beta\gamma\delta}(\Omega) = \eta_0(\Omega) \mathcal{P}_{\alpha\beta\gamma\delta}, \quad (35)$$

with the projector

$$\mathcal{P}_{\alpha\beta\gamma\delta} = \delta_{\alpha\gamma}\delta_{\beta\delta} + \delta_{\alpha\delta}\delta_{\beta\gamma} - \frac{2}{d}\delta_{\alpha\beta}\delta_{\gamma\delta}, \quad (36)$$

and  $d = 2$ . The scalar function  $\eta_0(\Omega)$  can be written as

$$\eta_0(\Omega) = \frac{N_f}{128} \left( \frac{\Omega}{v_H \sqrt{1 - \beta^2}} \right)^2, \quad (37)$$

which coincides with the tilt-free Hermitian form upon the identification  $v_F = v_H \sqrt{1 - \beta^2}$ . Thus, together with the QGT, the shear viscosity separates NH-insensitive optical probes from stress-sensitive observables that access effective non-Hermiticity in the real-spectrum weak-NH regime.

## VI. DISCUSSION AND CONCLUSIONS

A recurring difficulty in weakly non-Hermitian Dirac systems at charge neutrality is that many bulk responses can appear “Hermitian-like,” because the non-Hermitian coupling can often be absorbed into renormalized band parameters (most notably an effective Dirac velocity), obscuring independent access to the non-Hermitian strength. Our central message is that minimal Hamiltonian deformations act as a controlled filter: they separate observables fixed mainly by the dispersion from those that depend on how the eigenstates are deformed, and therefore reveal effective non-Hermiticity beyond a mere renormalization of band parameters. See also Table I.

This separation is already apparent across the hierarchy of bulk probes. The DOS remains linear,  $\rho(E) \sim |E|$ , but its slope distinguishes the two deformations: for type-I tilt it acquires an intrinsically NH-dependent contribution that cannot be absorbed into a single effective velocity [Eq. (13)], whereas for the VAD the result reduces to the standard anisotropic-Dirac form  $\rho \sim |E|/(v_x^{\text{eff}} v_y^{\text{eff}})$  with all  $\beta$ -dependence absorbed into effective velocities [Eq. (15)]. A complementary wave-function benchmark is provided by the biorthogonal QGT: the quantum metric is NH-insensitive for both deformations, being unchanged for tilt [Eq. (17)] and reducible to an anisotropic rescaling for VAD [Eq. (18)]. Consistently, the collisionless optical conductivities serve as robust NH-insensitive benchmarks: the linear response is universal for tilt [Eq. (23)] and maps onto the usual anisotropic-Dirac form for VAD under  $v_{x,y} \rightarrow v_{x,y}^{\text{eff}}$  [Eq. (24)], in line with optical sum rules linking interband optical weight to ground-state geometry [74–77]; at second order, symmetry selects a nonzero signal only for inversion-breaking tilt [Eqs. (28), (29)]. By contrast, the shear viscosity sharply differentiates the deformations: it collapses to an isotropic projector structure for tilt [Eqs. (35)–(37)], but for VAD it develops inequivalent tensor components with NH-dependent amplitudes [Eq. (34)], thereby singling out the DOS (tilt) and viscoelastic response (VAD) as the cleanest channels where minimal deformations prevent NH effects from being fully absorbed into parameter redefinitions.

A unifying outcome of our analysis is that, within the real-spectrum weak-NH regime, non-Hermiticity does not alter the leading power-law scaling of the observables considered here, which is fixed solely by the Dirac dynamic exponent  $z = 1$  and spatial dimensionality  $d = 2$ . Instead, it enters through response-dependent amplitudes and tensor structures. Depending on the probe, NH effects are either fully captured by effective parameter redefinitions or leave irreducible signatures in terms of NH-dependent prefactors, anisotropies, or symmetry-selected components that provide a detectable measure of effective non-Hermiticity.

At present, the most experimentally available Dirac-type non-Hermitian platforms are topoelectrical, photonic and ultracold atom realizations, where gain–loss and non-reciprocity can be engineered with considerable flexibility and where the minimal deformations considered here (tilt and velocity anisotropy) can be implemented in a controlled manner [78–82]. A practical advantage of these platforms is that both the spectrum and spatial mode profiles are directly accessible, enabling straightforward measurements of DOS analogues and wave-function diagnostics even in regimes where standard bulk responses would otherwise appear effectively Hermitian-like. By contrast, in metamaterial implementations (topoelectrical circuits and photonic lattices) the directly measured observables are effective linear-response functions of the engineered lattice model, rather than electronic transport coefficients such as charge optical conductivity or shear viscosity as in crystalline solids. In topoelectrical circuits, the natural observable is the complex, frequency-dependent impedance matrix (equivalently, the inverse circuit Laplacian), including nonlocal impedances that reveal boundary resonances and bulk spectral features in close analogy to Green’s-function diagnostics [83, 84]. In photonic platforms, frequency-resolved absorption plays an analogous role; related protocols can reconstruct both real and imaginary parts of *non-Hermitian spectra* in momentum space [85]. Ultracold atoms offer a complementary route in which non-Hermiticity is engineered via controlled dissipation: in a momentum-space lattice, a dissipative Aharonov–Bohm chain has been realized that exhibits the NHSE, with Bragg spectroscopy resolving endpoint modes [86]. This approach is expected to provide a natural pathway toward two-dimensional NH Dirac platforms. Beyond edge spectroscopy, closely related analogues of our bulk probes can be accessed through current response [87], circular-drive depletion (quantized dichroism) [88], and multi-tone rectification protocols [89].

Several extensions follow naturally. A promising direction is to extend the analysis beyond the clean, charge-neutral, collisionless regime, and investigate how the responses are modified once finite chemical potential and temperature, as well as disorder and interactions, introduce intraband processes and finite broadening [90, 91]. Likewise, entering the overtilted (type-II) regime should markedly modify both optical and viscoelastic response structures. Finally, extending the present frame-

work to three-dimensional Weyl systems, to collision-dominated (hydrodynamic) regimes, and to stronger non-Hermiticity where the spectrum becomes complex and exceptional structures emerge are all promising directions for future work.

## ACKNOWLEDGMENTS

We are grateful to Bitan Roy for the critical reading of the manuscript. This work was supported by Fondecyt (Chile) Grant No. 1230933 (V.J.). J.P.E. acknowl-

edges support from Agencia Nacional de Investigación y Desarrollo (ANID) – Scholarship Program through the Doctorado Nacional Grant No. 2024-21240412.

## Appendix A: Nonlinear optical conductivity: evaluation of $\chi^{(2)}$

In this appendix, we present the details of the calculation of nonlinear optical conductivity, which is related to the second-order susceptibility  $\chi_{ijk}^{(2)}(i\Omega_1, i\Omega_2)$ , with the corresponding Feynman diagram in Fig. 2, where

$$\chi_{ijk}^{(2)}(i\Omega_1, i\Omega_2) = \sum_{\mathcal{P}} \int \frac{d\omega}{2\pi} \int \frac{d^2\mathbf{k}}{(2\pi)^2} \text{Tr}\{J_i G_f(i\omega, \mathbf{k}) J_j G_f(i\omega + i\Omega_1, \mathbf{k}) J_k G_f(i\omega + i\Omega_1 + i\Omega_2, \mathbf{k})\} \quad (\text{A1})$$

For this, we will show the details of the calculation of the  $\chi_{yxy}^{(2)}(i\Omega_1, i\Omega_2)$  for the antisymmetric tilt case, showing that this method serves for all other components of the tensor. After completing the trace and integrating over the frequencies using residues, we obtain:

$$\begin{aligned} \chi_{yxy}^{(2)}(i\Omega_1, i\Omega_2) = & 4e^3 v_H^3 (1 - \beta^2)^{3/2} \sum_{\mathcal{P}} \int \frac{dk d\varphi}{(2\pi)^2} k \cos(\varphi) \left( 8(\beta^2 - 1)^2 k^4 v_H^4 (3 \cos(2\varphi) - 1) \right. \\ & + 8i\alpha(1 - \beta^2) k^3 (\Omega_1 + 2\Omega_2) v_H^3 \cos(\varphi) + 2(1 - \beta^2) k^2 v_H^2 (2\Omega_1^2 \cos^2(\varphi) + \Omega_2 \Omega_1 (\cos(2\varphi) - 3) + \Omega_2^2 (\cos(2\varphi) - 3)) \\ & \left. - 2i\alpha k \Omega_1^2 (\Omega_1 + 2\Omega_2) v_H \cos(\varphi) - \Omega_1^2 \Omega_2 (\Omega_1 + \Omega_2) \right) \\ & \times \frac{1}{(2\varepsilon_k - i\Omega_1)(2\varepsilon_k + i\Omega_1)(2\varepsilon_k - i\Omega_2)(2\varepsilon_k + i\Omega_2)(2\varepsilon_k - i(\Omega_1 + \Omega_2))(2\varepsilon_k + i(\Omega_1 + \Omega_2))} \end{aligned} \quad (\text{A2})$$

where  $\varepsilon_k = \sqrt{1 - \beta^2} k v_H$ . Now, we perform the analytical continuation  $i\Omega_m \rightarrow \omega_m + i\delta$ , and perform the partial fraction decomposition of the last factor to find

$$\int dk d\varphi \frac{f(k, \omega_m)}{\omega_m - \varepsilon_k + i\delta} = \int dk d\varphi f(k, \omega_m) (( - i\pi\delta(\omega_m - \varepsilon_k) + \mathcal{P}((\omega_m - \varepsilon_k))) \quad (\text{A3})$$

after carrying out the analytical continuation. Subsequently, integration over the delta functions yields

$$\chi_{yxy}^{(2)}(i\Omega_m \rightarrow \omega_m) = \sum_{\mathcal{P}} -\frac{iN_f e^3 \alpha v_H}{16} \quad (\text{A4})$$

Now, we carry out the sum over the permutation  $\omega_1 \rightarrow \omega_2$ , and obtain the second order linear conductivity:

$$\sigma_{yxy}^{(2)}(\omega_1, \omega_2) = - \sum'_{\mathcal{P}} \frac{\chi_{yxy}^{(2)}(i\Omega_1, i\Omega_2)}{\omega_1 \omega_2} \Big|_{i\Omega_m \rightarrow \omega_m + i\delta} \quad (\text{A5})$$

$$\sigma_{yxy}^{(2)}(\omega_1, \omega_2) = -\frac{iN_f e^3 \alpha v_H}{8\omega_1 \omega_2} \quad (\text{A6})$$

For the  $xxx$  and  $xyy$  components, we find

$$\chi_{xxx}^{(2)}(i\Omega_m \rightarrow \omega_m) = \chi_{xyy}^{(2)} = N_f \sum_{\mathcal{P}} -\frac{i\alpha e^3 (\omega_1 - \omega_2) v_H}{4(\omega_1 + \omega_2)} \quad (\text{A7})$$

When we sum over frequencies, due to its antisymmetry, both components vanish,

$$\sigma_{xxx}^{(2)}(\omega_1, \omega_2) = \sigma_{xyy}^{(2)}(\omega_1, \omega_2) = 0. \quad (\text{A8})$$

## Appendix B: Viscosity tensor for the velocity-anisotropy deformation

We here show the explicit expressions for the three independent dimensionless scaling functions  $f_{1,2,3}(\alpha, \beta, \Omega)$  for the components of the viscosity tensor in the case of the VAD, as given by the scaling form in Eq. (34). They

can be expressed in terms of complete elliptic integrals

$K(m)$  and  $E(m)$  as follows:

---


$$f_1(\alpha, \beta, \Omega) = \frac{N_f}{48\pi\alpha^4 v_H} \left( \sqrt{1-\beta^2} (\alpha^2 - 2\beta^2 + 2) E\left(\frac{\alpha^2}{\beta^2-1}\right) + (\alpha^2 - 2\beta^2 + 2) \sqrt{\alpha^2 - \beta^2 + 1} E\left(\frac{\alpha^2}{\alpha^2 - \beta^2 + 1}\right) \right. \\ \left. + 2\sqrt{1-\beta^2} (-\alpha^2 + \beta^2 - 1) K\left(\frac{\alpha^2}{\beta^2-1}\right) + 2(\beta^2 - 1) \sqrt{\alpha^2 - \beta^2 + 1} K\left(\frac{\alpha^2}{\alpha^2 - \beta^2 + 1}\right) \right), \quad (B1)$$

$$f_2(\alpha, \beta, \Omega) = \frac{N_f}{48\pi\alpha^4(\beta^2-1)(\alpha^2-\beta^2+1)^{3/2} v_H} \left[ \sqrt{(\beta^2-1)(-\alpha^2+\beta^2-1)} E\left(\frac{\alpha^2}{\beta^2-1}\right) \right. \\ \times \left( 8\alpha^2(\beta^2-1)^2 - 2(\beta^2-1)^3 - 2\alpha^6 - \alpha^4(\beta^2-1) \right) \\ - (\alpha^2 - \beta^2 + 1) \left( \alpha^4 + 7\alpha^2(\beta^2-1) - 2(\beta^2-1)^2 \right) (\beta^2-1) K\left(\frac{\alpha^2}{\alpha^2 - \beta^2 + 1}\right) \\ - \sqrt{(\beta^2-1)(-\alpha^2+\beta^2-1)} K\left(\frac{\alpha^2}{\beta^2-1}\right) \\ \left. - (\alpha^2 - \beta^2 + 1) \left( 2\alpha^6 + \alpha^4(\beta^2-1) - 8\alpha^2(\beta^2-1)^2 + 2(\beta^2-1)^3 \right) E\left(\frac{\alpha^2}{\alpha^2 - \beta^2 + 1}\right) \right], \quad (B2)$$

$$f_3(\alpha, \beta, \Omega) = \frac{N_f}{48\pi\alpha^4\sqrt{1-\beta^2}(-\alpha^2+\beta^2-1)v_H} \left[ 3(\beta^2-1) \left( 3\alpha^4 - 2\alpha^2(\beta^2-1) - 2(\beta^2-1)^2 \right) E\left(\frac{\alpha^2}{\beta^2-1}\right) \right. \\ - \alpha^2(3\alpha^2 + \beta^2 - 1) \sqrt{-(\alpha^2+2)\beta^2 + \alpha^2 + \beta^4 + 1} K\left(\frac{\alpha^2}{\alpha^2 - \beta^2 + 1}\right) \\ + \left( 6\alpha^6 - 13\alpha^4(\beta^2-1) + \alpha^2(\beta^2-1)^2 + 6(\beta^2-1)^3 \right) K\left(\frac{\alpha^2}{\beta^2-1}\right) \\ \left. + \left( 3\alpha^4 - 2\alpha^2(\beta^2-1) - 2(\beta^2-1)^2 \right) \text{Im} \left\{ \alpha^2 K\left(\frac{-\alpha^2 + \beta^2 - 1}{\beta^2-1}\right) - (\beta^2-1) E\left(\frac{-\alpha^2 + \beta^2 - 1}{\beta^2-1}\right) \right\} \right]. \quad (B3)$$


---

- [1] R. El-Ganainy, K. G. Makris, M. Khajavikhan, Z. H. Musslimani, S. Rotter, and D. N. Christodoulides, Non-hermitian physics and PT symmetry, *Nature Physics* **14**, 11 (2018).
- [2] Y. Ashida, Z. Gong, and M. Ueda, Non-hermitian physics, *Advances in Physics* **69**, 249 (2020).
- [3] E. J. Bergholtz, J. C. Budich, and F. K. Kunst, Exceptional topology of non-hermitian systems, *Reviews of Modern Physics* **93**, 015005 (2021).
- [4] M.-A. Miri and A. Alù, Exceptional points in optics and photonics, *Science* **363**, eaar7709 (2019).
- [5] V. Jurićić and B. Roy, Yukawa-lorentz symmetry in non-hermitian dirac materials, *Communications Physics* **7**, 169 (2024).
- [6] S. A. Murshed and B. Roy, Quantum electrodynamics of non-hermitian dirac fermions, *Journal of High Energy Physics* **2024**, 1 (2024).
- [7] X.-J. Yu, Z. Pan, L. Xu, and Z.-X. Li, Non-hermitian strongly interacting dirac fermions, *Phys. Rev. Lett.* **132**, 116503 (2024).
- [8] S. A. Murshed and B. Roy, Yukawa-lorentz symmetry

of interacting non-hermitian birefringent dirac fermions, *SciPost Phys.* **18**, 073 (2025).

- [9] C. A. Leong and B. Roy, Amplified magnetic catalysis in non-hermitian euclidean and hyperbolic dirac liquids (2025), [arXiv:2510.02304 \[cond-mat.str-el\]](https://arxiv.org/abs/2510.02304).
- [10] B. Roy, Zero modes and index theorems for non-hermitian dirac fermions, *Phys. Rev. D* **112**, 125016 (2025).
- [11] J. P. Esparza and V. Jurićić, Exceptional magic angles in non-hermitian twisted bilayer graphene, *Phys. Rev. Lett.* **134**, 226602 (2025).
- [12] A. H. Castro Neto, F. Guinea, N. M. R. Peres, K. S. Novoselov, and A. K. Geim, The electronic properties of graphene, *Reviews of Modern Physics* **81**, 109 (2009).
- [13] N. P. Armitage, E. J. Mele, and A. Vishwanath, Weyl and dirac semimetals in three-dimensional solids, *Reviews of Modern Physics* **90**, 015001 (2018).
- [14] M. Polini, F. Guinea, M. Lewenstein, H. C. Manoharan, and V. Pellegrini, Artificial honeycomb lattices for electrons, atoms and photons, *Nature Nanotechnology* **8**, 625 (2013).

[15] L. Tarruell, D. Greif, T. Uehlinger, G. Jotzu, and T. Esslinger, Creating, moving and merging dirac points with a fermi gas in a tunable honeycomb lattice, *Nature* **483**, 302 (2012).

[16] Y. Plotnik, O. Peleg, F. Dreisow, M. Heinrich, S. Nolte, A. Szameit, and M. Segev, Observation of unconventional edge states in photonic graphene, *Nature Materials* **13**, 57 (2014).

[17] V. M. Martinez Alvarez, J. E. Barrios Vargas, and L. E. F. Foa Torres, Non-hermitian robust edge states in one dimension: Anomalous localization and eigenspace condensation at exceptional points, *Phys. Rev. B* **97**, 121401 (2018).

[18] S. Yao and Z. Wang, Edge states and topological invariants of non-hermitian systems, *Phys. Rev. Lett.* **121**, 086803 (2018).

[19] C. H. Lee and R. Thomale, Anatomy of skin modes and topology in non-hermitian systems, *Phys. Rev. B* **99**, 201103 (2019).

[20] D. S. Borgnia, A. J. Kruchkov, and R.-J. Slager, Non-hermitian boundary modes and topology, *Phys. Rev. Lett.* **124**, 056802 (2020).

[21] K. Zhang, Z. Yang, and C. Fang, Correspondence between winding numbers and skin modes in non-hermitian systems, *Phys. Rev. Lett.* **125**, 126402 (2020).

[22] N. Okuma, K. Kawabata, K. Shiozaki, and M. Sato, Topological origin of non-hermitian skin effects, *Phys. Rev. Lett.* **124**, 086801 (2020).

[23] D. J. Salib, S. K. Das, and B. Roy, Model non-hermitian topological operators without skin effect (2023), arXiv:2309.12310 [cond-mat.mes-hall].

[24] N. Okuma, K. Kawabata, K. Shiozaki, and M. Sato, Topological origin of non-hermitian skin effects, *Phys. Rev. Lett.* **124**, 086801 (2020).

[25] K. Zhang, Z. Yang, and C. Fang, Universal non-hermitian skin effect in two and higher dimensions, *Nat. Commun.* **13**, 2496 (2022).

[26] J. H. D. Rivero, L. Feng, and L. Ge, Imaginary gauge transformation in momentum space and dirac exceptional point, *Phys. Rev. Lett.* **129**, 243901 (2022).

[27] H. Hu, Topological origin of non-hermitian skin effect in higher dimensions and uniform spectra, *Science Bulletin* **70**, 51 (2025).

[28] W. D. Heiss, The physics of exceptional points, *J. Phys. A: Math. Theor.* **45**, 444016 (2012).

[29] K. Kawabata, T. Bessho, and M. Sato, Classification of exceptional points and non-hermitian topological semimetals, *Phys. Rev. Lett.* **123**, 066405 (2019).

[30] D. C. Brody, Biorthogonal quantum mechanics, *J. Phys. A: Math. Theor.* **47**, 035305 (2014).

[31] F. K. Kunst, E. Edvardsson, J. C. Budich, and E. J. Bergholtz, Biorthogonal bulk-boundary correspondence in non-hermitian systems, *Phys. Rev. Lett.* **121**, 026808 (2018).

[32] M. O. Goerbig, J.-N. Fuchs, G. Montambaux, and F. Piéchon, Tilted anisotropic dirac cones in quinoid-type graphene and  $\alpha$ -(BEDT-TTF)<sub>2</sub>i<sub>3</sub>, *Phys. Rev. B* **78**, 045415 (2008).

[33] M. Trescher, B. Sbierski, P. W. Brouwer, and E. J. Bergholtz, Quantum transport in dirac materials: Signatures of tilted and anisotropic dirac and weyl cones, *Phys. Rev. B* **91**, 115135 (2015).

[34] A. Varykhalov, D. Marchenko, J. Sánchez-Barriga, E. Golias, O. Rader, and G. Bihlmayer, Tilted dirac cone on w(110) protected by mirror symmetry, *Phys. Rev. B* **95**, 245421 (2017).

[35] G. E. Volovik and K. Zhang, Lifshitz transitions, type-ii dirac and weyl fermions, event horizon and all that, *Journal of Low Temperature Physics* **189**, 276 (2017).

[36] T. S. Sikkens and L. Fritz, Disorder in tilted weyl semimetals from a renormalization group perspective, *Phys. Rev. B* **96**, 155121 (2017).

[37] P. Reiser and V. Juričić, Tilted dirac superconductor at quantum criticality: restoration of lorentz symmetry, *Journal of High Energy Physics* **2024**, 1 (2024).

[38] H. Hu and F. Krüger, Quantum criticality of type-i and critically tilted dirac semimetals, *Physica C: Superconductivity and its Applications* **632**, 1354687 (2025).

[39] C.-Y. Moon, J. Han, H. Lee, and H. J. Choi, Low-velocity anisotropic dirac fermions on the side surface of topological insulators, *Phys. Rev. B* **84**, 195425 (2011).

[40] Z. K. Liu, B. Zhou, Y. Zhang, Z. J. Wang, H. M. Weng, D. Prabhakaran, S.-K. Mo, Z. X. Shen, Z. Fang, X. Dai, *et al.*, Discovery of a three-dimensional topological dirac semimetal, na<sub>3</sub>bi, *Science* **343**, 864 (2014).

[41] Z. K. Liu, J. Jiang, B. Zhou, Z. J. Wang, Y. Zhang, H. M. Weng, D. Prabhakaran, S. K. Mo, H. Peng, P. Dudin, *et al.*, A stable three-dimensional topological dirac semimetal cd<sub>3</sub>as<sub>2</sub>, *Nature Materials* **13**, 677 (2014).

[42] Y. I. Rodionov, K. I. Kugel, and F. Nori, Effects of anisotropy and disorder on the conductivity of weyl semimetals, *Phys. Rev. B* **92**, 195117 (2015).

[43] D. Mastrogiovanni, N. Sandler, and S. E. Ulloa, Hybridization and anisotropy in the exchange interaction in three-dimensional dirac semimetals, *Phys. Rev. B* **93**, 094433 (2016).

[44] O. Pozo, Y. Ferreiros, and M. A. H. Vozmediano, Anisotropic fixed points in dirac and weyl semimetals, *Phys. Rev. B* **98**, 115122 (2018).

[45] W. Ma, Z. Yang, D. Ma, Z. Lv, and Z. Liu, Prediction of a two-dimensional anisotropic dirac semimetal carbon allotrope with high strength and quasi-one-dimensional transport, *Phys. Rev. B* **112**, 094111 (2025).

[46] J.-P. Provost and G. Vallée, Riemannian structure on manifolds of quantum states, *Commun. Math. Phys.* **76**, 289 (1980).

[47] H. Shen, B. Zhen, and L. Fu, Topological band theory for non-hermitian hamiltonians, *Phys. Rev. Lett.* **120**, 146402 (2018).

[48] T. Ozawa, Steady-state hall response and quantum geometry of driven-dissipative lattices, *Phys. Rev. B* **97**, 041108 (2018).

[49] D.-J. Zhang, Q.-h. Wang, and J. Gong, Quantum geometric tensor in  $\mathcal{PT}$ -symmetric quantum mechanics, *Phys. Rev. A* **99**, 042104 (2019).

[50] Q. Zhang and B. Wu, Non-hermitian quantum systems and their geometric phases, *Phys. Rev. A* **99**, 032121 (2019).

[51] Y.-Q. Zhu, W. Zheng, S.-L. Zhu, and G. Palumbo, Band topology of pseudo-hermitian phases through tensor berry connections and quantum metric, *Phys. Rev. B* **104**, 205103 (2021).

[52] D. D. Solnyshkov, C. Leblanc, L. Bessonart, A. Nalitov, J. Ren, Q. Liao, F. Li, and G. Malpuech, Quantum metric and wave packets at exceptional points in non-hermitian systems, *Phys. Rev. B* **103**, 125302 (2021).

[53] Y.-M. R. Hu, E. A. Ostrovskaya, and E. Estrecho, Generalized quantum geometric tensor in a non-hermitian

exciton-polariton system [invited], *Opt. Mater. Express* **14**, 664 (2024).

[54] T. Ozawa and H. Schomerus, Geometric contribution to adiabatic amplification in non-hermitian systems, *Phys. Rev. Res.* **7**, 013173 (2025).

[55] A. H. Castro Neto, F. Guinea, N. M. R. Peres, K. S. Novoselov, and A. K. Geim, The electronic properties of graphene, *Rev. Mod. Phys.* **81**, 109 (2009).

[56] S. Pino-Alarcón and V. Jurićić, Yukawa-lorentz symmetry of tilted non-hermitian dirac semimetals at quantum criticality, *Phys. Rev. B* **111**, 195126 (2025).

[57] M. V. Berry, Quantal phase factors accompanying adiabatic changes, *Proc. R. Soc. Lond. A* **392**, 45 (1984).

[58] J. C. Garrison and E. M. Wright, Complex geometrical phases for dissipative systems, *Phys. Lett. A* **128**, 177 (1988).

[59] Y. Ulrich, J. Mitscherling, L. Classen, and A. P. Schnyder, *Quantum geometric origin of the intrinsic nonlinear hall effect* (2025), arXiv:2506.17386 [cond-mat.mes-hall].

[60] S. Sachdev, *Quantum Phase Transitions*, 2nd ed. (Cambridge University Press, Cambridge, UK, 2011).

[61] C. Aversa and J. E. Sipe, Nonlinear optical susceptibilities of semiconductors: Results with a length-gauge analysis, *Phys. Rev. B* **52**, 14636 (1995).

[62] T. Morimoto and N. Nagaosa, Topological nature of nonlinear optical effects in solids, *Phys. Rev. B* **94**, 035117 (2016).

[63] H. Rostami and V. Jurićić, Probing quantum criticality using nonlinear hall effect in a metallic dirac system, *Phys. Rev. Res.* **2**, 013069 (2020).

[64] T. Morimoto and N. Nagaosa, Topological nature of nonlinear optical effects in solids, *Science Advances* **2**, e1501524 (2016).

[65] I. V. Tokatly and G. Vignale, Lorentz shear modulus of a two-dimensional electron gas at high magnetic field, *Phys. Rev. B* **76**, 161305(R) (2007).

[66] B. Bradlyn, M. Goldstein, and N. Read, Kubo formulas for viscosity: Hall viscosity, spin density, and torsion, *Physical Review B* **86**, 245309 (2012).

[67] M. Müller, L. Fritz, and S. Sachdev, Quantum-critical relativistic magnetotransport in graphene, *Phys. Rev. B* **78**, 115406 (2008).

[68] I. Torre, A. Tomadin, A. K. Geim, and M. Polini, Non-local transport and the hydrodynamic shear viscosity in graphene, *Phys. Rev. B* **92**, 165433 (2015).

[69] A. Eberlein, A. A. Patel, and S. Sachdev, Transport in clean two-dimensional dirac systems: Hydrodynamic and ballistic regimes, *Physical Review B* **95**, 075127 (2017).

[70] J. M. Link, D. E. Sheehy, B. N. Narozhny, and J. Schmalian, Viscosity and hydrodynamic transport in graphene: Interaction effects and nonlocal response, *Physical Review B* **98**, 195103 (2018).

[71] J. M. Link, B. N. Narozhny, E. I. Kiselev, and J. Schmalian, Out-of-equilibrium hydrodynamic transport in dirac fluids, *Physical Review Letters* **120**, 196801 (2018).

[72] C. Copetti and K. Landsteiner, Viscosity in dirac fluids and holographic bounds, *Physical Review B* **99**, 195146 (2019).

[73] M. Moore, P. Surówka, V. Jurićić, and B. Roy, Shear viscosity as a probe of nodal topology, *Phys. Rev. B* **101**, 161111 (2020).

[74] R. Resta and S. Sorella, Electron localization in the insulating state, *Physical Review Letters* **82**, 370 (1999).

[75] I. Souza, T. Wilkens, and R. M. Martin, Polarization and localization in insulators: Generating function approach, *Physical Review B* **62**, 1666 (2000).

[76] N. Verma and R. Queiroz, Instantaneous response and quantum geometry of insulators, *Proceedings of the National Academy of Sciences of the United States of America* **122**, e2405837122 (2025).

[77] R. Resta, Nonadiabatic quantum geometry and optical conductivity, *Physical Review B* **111**, 205107 (2025).

[78] X. Zhang, C. Wu, M. Yan, N. Liu, Z. Wang, and G. Chen, Observation of continuum landau modes in non-hermitian electric circuits, *Nature Communications* **15**, 1798 (2024).

[79] P. Zhu, X.-Q. Sun, T. L. Hughes, and G. Bahl, Higher rank chirality and non-hermitian skin effect in a topoelectrical circuit, *Nature Communications* **14**, 720 (2023).

[80] X. Xie, F. Ma, W. B. Rui, *et al.*, Non-hermitian dirac cones with valley-dependent lifetimes, *Nature Communications* **16**, 1627 (2025).

[81] L. Yu, H. Xue, R. Guo, E. A. Chan, Y. Y. Terh, C. Soci, B. Zhang, and Y. D. Chong, Dirac mass induced by optical gain and loss, *Nature* **632**, 63 (2024).

[82] B. Zhen, C.-W. Hsu, Y. Igarashi, *et al.*, Spawning rings of exceptional points out of dirac cones, *Nature* **525**, 354 (2015).

[83] C. H. Lee, S. Imhof, C. Berger, F. Bayer, J. Brehm, L. W. Molenkamp, T. Kiessling, and R. Thomale, Topoelectrical circuits, *Communications Physics* **1**, 39 (2018).

[84] H. Sahin, M. B. A. Jalil, and C. H. Lee, Topoelectrical circuits—recent experimental advances and developments, *APL Electronic Devices* **1**, 021503 (2025).

[85] K. Li and Y. Xu, Non-hermitian absorption spectroscopy, *Physical Review Letters* **129**, 093001 (2022).

[86] Q. Liang, D. Xie, Z. Dong, H. Li, H. Li, B. Gadway, W. Yi, and B. Yan, Dynamic signatures of non-hermitian skin effect and topology in ultracold atoms, *Physical Review Letters* **129**, 070401 (2022).

[87] R. Anderson, F. Wang, P. Xu, V. Venu, S. Trotzky, F. Chevy, and J. H. Thywissen, Conductivity spectrum of ultracold atoms in an optical lattice, *Physical Review Letters* **122**, 153602 (2019).

[88] L. Asteria, D. T. Tran, T. Ozawa, M. Tarnowski, B. S. Rem, N. Fläschner, K. Sengstock, N. Goldman, and C. Weitenberg, Measuring quantized circular dichroism in ultracold topological matter, *Nature Physics* **15**, 449 (2019).

[89] E. Lundh and M. Wallin, Ratchet effect for cold atoms in an optical lattice, *Physical Review Letters* **94**, 110603 (2005).

[90] J. Nissinen and G. E. Volovik, Type-iii and iv interacting weyl points, *JETP Letters* **105**, 447 (2017).

[91] V. Kozii and L. Fu, Non-hermitian topological theory of finite-lifetime quasiparticles, *Physical Review B* **109**, 235139 (2024).